Current distribution measurements inside an electromagnetic plasma gun operated in a gas-puff mode

Cite as: Phys. Plasmas **17**, 123508 (2010); https://doi.org/10.1063/1.3526603
Submitted: 10 September 2010 . Accepted: 22 November 2010 . Published Online: 28 December 2010

Flavio R. Poehlmann, Mark A. Cappelli, and Gregory B. Rieker

Current distribution measurements inside an electromagnetic plasma gun operated in a gas-puff mode

Flavio R. Poehlmann,[1] Mark A. Cappelli,[1] and Gregory B. Rieker[2]
[1]*Department of Mechanical Engineering, Stanford University, Stanford, California 94305, USA*
[2]*Fluence, LLC, 37444 Sycamore Street, Unit 16, Newark, California 94560, USA*

(Received 10 September 2010; accepted 22 November 2010; published online 28 December 2010)

Measurements are presented of the time-dependent current distribution inside a coaxial electromagnetic plasma gun. The measurements are carried out using an array of six axially distributed dual-Rogowski coils in a balanced circuit configuration. The radial current distributions indicate that operation in the gas-puff mode, i.e., the mode in which the electrode voltage is applied before injection of the gas, results in a stationary ionization front consistent with the presence of a plasma deflagration. The effects of varying the bank capacitance, transmission line inductance, and applied electrode voltage were studied over the range from 14 to 112 μF, 50 to 200 nH, and 1 to 3 kV, respectively. © *2010 American Institute of Physics*. [doi:10.1063/1.3526603]

I. INTRODUCTION

Pulsed coaxial plasma guns are of interest in a variety of applications, such as plasma-injection into fusion machines,[1–3] dense plasma focus devices for neutron and x-ray production,[4–6] plasma ion implantation in materials processing,[7,8] and in space plasma propulsion.[9,10] In several of these applications, the filling of the coaxial gun with process gas precedes the breakdown process, resulting in the formation of an ionization zone (current sheet) that propagates as a result of the $\boldsymbol{J}\times\boldsymbol{B}$ forces, pushing on the neutral gas in front, thereby accelerating the combination of ionized and neutral gas to high velocities.[11] Because of this interaction between the current sheet and unprocessed gas, operation in this prefilled mode is often referred to as the "snowplow" mode in the vast literature.[11–13]

A less common mode, sometimes referred to as the "high energy mode,"[5] or, as we refer to here, as the "gas-puff mode" is entered when the electrode voltage is applied *before* injection of the gas. In this mode, the gas is concentrated near the breech of the gun when the breakdown initiates. It has been reported by several researchers[14,15] that a plasma gun operating in this gas-puff as opposed to the prefill method of gas introduction does not operate in a snowplow mode. Instead, it is characterized by a stationary ionization zone that is located at the upstream (breech) end of the gun followed by a downstream current conduction region that accelerates plasma by continuously processing (ionizing) injected neutral gas. In analogy to a similar operating mode in chemical combustion, this mode of operation has been introduced by Cheng[14] as a plasma deflagration mode. A plasma gun operated in this gas-puff mode is sometimes referred to as a plasma deflagration gun.[14–16]

The primary objective of the study reported here is to characterize the dynamics of the current distribution within the interior of a coaxial plasma gun operating in a gas-puff mode. Of particular interest is that higher exhaust velocities appear attainable for fixed circuit parameters and propellant mass[10,14,15] and that the negative effects of blowby/current sheet canting[11,17] may be less relevant to acceleration in a deflagration mode of operation.[18] For these reasons, a better understanding of the plasma deflagration mode may enable scaled plasma guns that could provide a high fluence of particles with kinetic energies that are several orders of magnitude higher. In addition, a secondary interest was in verifying that the operation of the plasma gun with a stationary ionization zone can be maintained over a range of relatively low voltages (1–3 kV), a regime of operation that is generally lower than that of prior coaxial gun studies. Since the compression and heating in the current sheet are avoided during the free expansion in a deflagration, a plasma gun operating in this regime has the potential to significantly improve the efficiency of electromagnetic pulsed plasma thrusters (PPTs) for space propulsion applications, and an extension of the operation to relatively low voltages is more suitable for the development of practical gas-fed PPTs. We also describe below a parametric study of the plasma gun behavior with varying circuit properties (bank capacitance and transmission line inductance).

Rogowski coils were used to measure the cathode currents at different axial locations. In addition, a fast framing camera capturing the visible light emission from the interior and downstream region of the plasma was correlated with the spatial Rogowski coil signatures to further discern the details in the dynamic plasma evolution within the discharge. While prior studies have also used immersed magnetic probes to characterize the deflagration to snowplow transition in similar coaxial guns,[14–16] they were of the B-dot variety, measuring the local magnetic field at a point off the axis of the discharge. B-dot probes are relatively simple in comparison to Rogowski coils, and, in principle, the current distribution within the plasma gun can be computed from a sufficient number of radially and axially distributed point measurements throughout the discharge, provided that the discharge is azimuthally symmetric. We chose instead to use distributed Rogowski coils, which are slightly more complicated in their design, but when placed around the central electrode (cathode, in our case), detect the current directly, without the need to assume azimuthal symmetry. Due to their larger size,

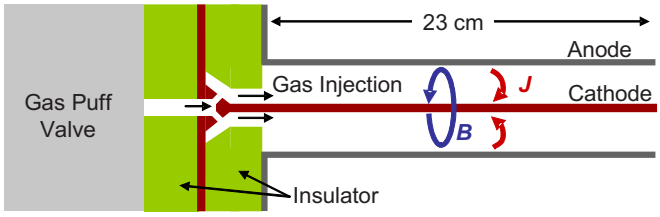

FIG. 1. (Color online) Schematic of the Stanford coaxial plasma gun.

Rogowski coils may be more intrusive than B-dot probes. However, images taken with the fast framing camera for operation with and without the current probes installed showed only minor changes in discharge behavior. This is briefly discussed in Sec. V. To our knowledge, direct measurements of current distribution using distributed Rogowski coils have not been previously reported in coaxial plasma guns operating in the deflagration mode.

The following section (Sec. II) describes the plasma gun and experimental setup in detail. Sections III and IV provide a review of Rogowski coil theory and describe the Rogowski coils that were designed and constructed for this study. Section V presents and analyzes the measured current distribution and fast framing camera images for operation with a bank capacitance of 112 μF, a transmission line inductance of 50 nH and an applied electrode voltage of 1 kV. As will be shown, these data confirm the existence of a stationary ionization front (deflagration). The effects of varying the capacitance, transmission line inductance, and applied electrode voltage on the dynamics of the deflagration are then presented in Sec. VI.

II. EXPERIMENT

Figure 1 shows a schematic of the coaxial plasma gun used in the experiments. The outer electrode (anode) had an inner radius of 2.5 cm, while the solid copper inner electrode (cathode) had an outer radius of 2.5 mm. Both electrodes were 23 cm long and were straight without taper. A rod-based design was chosen for the outer electrode to allow visual access to the interior of the plasma gun. The anode consisted of 15 stainless steel rods of 5 mm diameter that were arranged in a ring with 6.5 mm gaps between them.

A capacitor bank consisting of eight capacitors, each with a capacitance of 14 μF and a parasitic inductance of 15 nH, was connected directly to the gun electrodes using 1.75 m long RG-8 transmission lines, each with a parasitic inductance of approximately 400 nH. No switch was used in the experiments described here. Initially, voltage breakdown between the electrodes of the gun was held off on the vacuum side of the Paschen minimum. The discharge was then initiated by injecting a hydrogen gas-puff from a commercially available fast acting gas-puff valve (RM Jordan C-211).

Figure 2 shows a schematic of the experimental setup for measuring the current distribution inside the plasma gun. Six individual coil assemblies were constructed as described in detail in Sec. IV. Five of these coils were placed on top of a long copper tube that was inserted into the plasma gun, thereby positioning the coils axially around the cathode at locations 5, 10, 15, 20, and 25 cm from the gas injection entrance. The tube also served as a shielded conduit for the coil leads. The tube and coils were electrically insulated from the plasma using silicone rubber coated fiberglass sleeves. In addition, several layers of fiberglass insulating tape were used to electrically insulate the junctions between the coils and the conduit. The last of the six coil assemblies was placed around the return line of one of the transmission lines to infer the total cathode current at the 0 cm location. In order to reduce the number of required oscilloscope channels, only one coil assembly was placed on a single transmission line and its signal was multiplied by the number of transmission lines used. Since great care was taken to ensure that all transmission lines had exactly the same length, it was expected and confirmed experimentally that the current from the capacitors to the gun was split evenly across the identical RG-8 coaxial transmission lines. Each pair of Rogowski coils was connected to an electric circuit that integrated the signal. The specifics of the circuit are described in more detail below in Sec. IV.

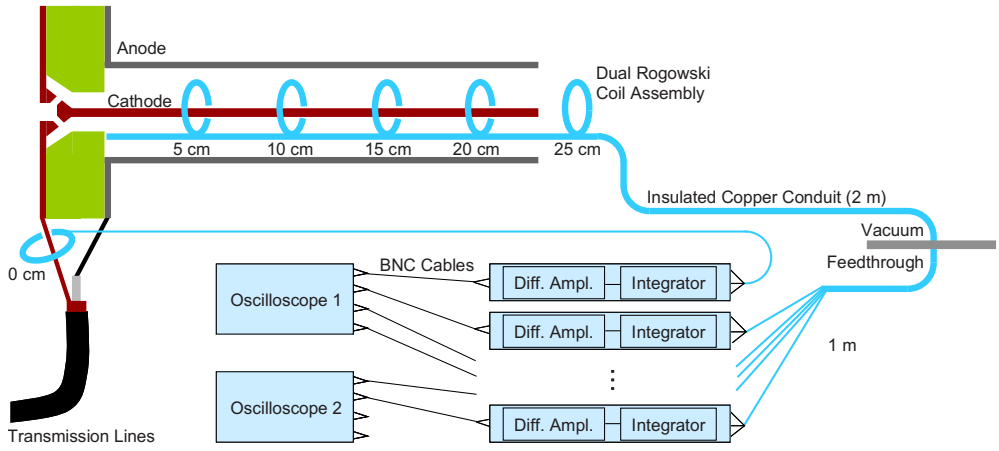

FIG. 2. (Color online) Schematic of experiment setup of axially distributed Rogowski coils for current distribution measurements.

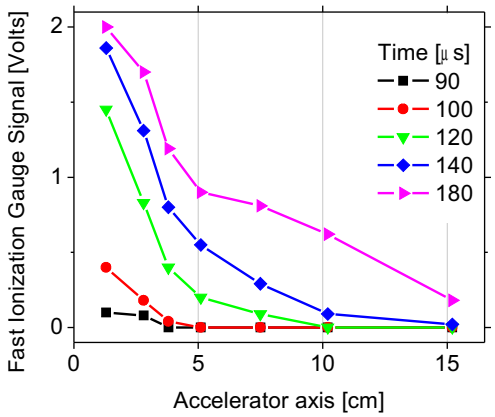

FIG. 3. (Color online) Axial distribution of gas density inside plasma gun at different times after triggering the gas puff valve.

A fast framing camera (Cordin Co., Model 222) was used to take a sequence of 16 images during the discharge pulse. The plasma gun was installed on one end of a 0.9 m long, 15 cm diameter Pyrex glass tube, the other end of which was connected to a large vacuum tank that provided a low background pressure of approximately 10^{-6} torr. The fast framing camera was placed at a distance of 3 m from the gun with its viewing angle aligned perpendicularly to the acceleration axis. With the exception of the first 5 cm of the gun, which were obstructed by the flange of the glass tube, the camera was able to capture the interior of the gun as well as the first 20 cm downstream of the gun exit plane. The trigger was provided from a separate Rogowski coil that was placed around the transmission line and triggered a TTL signal from a digital pulse generator (Stanford Research Systems DG 535). As a result, the $t=0$ reference point for all images was the breakdown event which initiated the plasma discharge.

The generated TTL signal was also used to track the delay between triggering the gas-puff valve and voltage breakdown. The recorded delay times varied between 75 and 120 μs. Figure 3 shows the axial gas density distribution inside the plasma gun at different times after gas injection, measured using an ac-coupled fast-ionization gauge (RM Jordan B-451). It can be deduced that breakdown occurred immediately as the gas entered the gun and that no significant amount of injected gas was downstream of the gun breech at the time of breakdown. This confirms that the gun operated in a gas-puff mode.

The mass flow entering the gun was estimated by normalizing the time-resolved pressure profile from the ac-coupled fast-ionization gauge against the total mass bit size, which had been determined before by measuring the pressure rise after gas injection into a known volume. It was found that the mass flow stabilized at approximately 8 mg/s at the time of breakdown and remained constant well beyond the duration of the discharge pulse. Given the 500 μm diameter of the nozzle and the 10 atm plenum pressure this would translate to a discharge coefficient for the choked nozzle of ~0.06 (i.e., an effective diameter of 120 μm). The initial temperature of the gas in the valve plenum was approximately 295 K (room temperature), but substantial cooling to a few tens of kelvin is expected as a result of the supersonic expansion into vacuum.[19] The operating parameters that could be varied on the valve were the plenum pressure and the amplitude of the current pulse that energized the valve. Both of these were set to their maximum settings (10 atm, 5000 A) in order to achieve maximum mass flow. At lower mass flow rates, noise on the current traces gradually increased and erosion at the cathode base became observable over ~100 shots, probably due to a starvation of charge carriers. Other effects on discharge behavior were not observable in the current waveforms and fast framing camera images. Hydrogen gas was chosen as the process gas, primarily to enable easy comparison to the prior work on deflagration guns performed by others.[14–16]

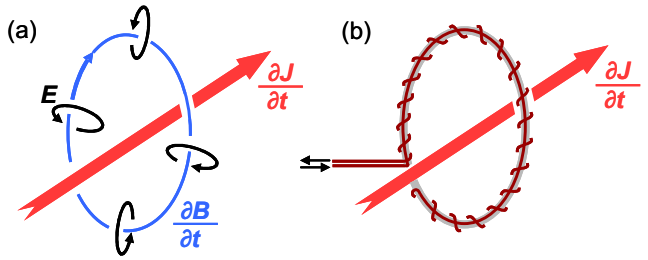

FIG. 4. (Color online) Principle of operation of a Rogowski coil. A time-varying current induces a combination of magnetic and electric fields (a), which induce a voltage in the minor windings of a Rogowski coil (b).

III. ROGOWSKI COIL THEORY

Rogowski coils generally consist of a toroidal solenoid that is wrapped around a conductor or conductive region. As illustrated in Fig. 4, Rogowski coil detection makes use of Ampere's law,

$$\vec{\nabla} \times \vec{B} = \mu_o \vec{J} + \mu_o \varepsilon_o \frac{\partial \vec{E}}{\partial t}, \tag{1}$$

which states that a current density, J, and time-varying field, E, induces an azimuthal magnetic field, B, around itself, and of Faraday's law,

$$\vec{\nabla} \times \vec{E} = -\frac{\partial \vec{B}}{\partial t}, \tag{2}$$

which states that any time-variation in the induced magnetic field induces an electric field azimuthally around the magnetic field lines. Here, ε_o and μ_o are the permittivity and permeability of free space, respectively. If the windings making up the Rogowski coil are oriented in such a way that they are aligned with the induced electric field lines, a signal is produced that is directly related to the enclosed current. This concept was first proposed by Chattock in 1887 (Ref. 20) and later further developed by Rogowski and Steinhaus.[21] While Rogowski coils generally are used on external circuit components, several researchers have successfully immersed them into energetic plasmas. Examples of such measurements include the studies by Wright[22] and Piperno *et al.*[23] on

plasma pinch devices. Although the general theory of Rogowski coils is widely accepted and well understood, not all of the information relevant to this study could be found in a single reference. Therefore, this section summarizes relevant aspects described in Refs. 22 and 24–26.

Using Stoke's theorem, Eq. (2) can be written in integral form as path and surface integrals, i.e.,

$$\oint_S \vec{E} \cdot d\vec{l} = -\frac{d}{dt}\oint_A \vec{B} \cdot d\hat{n}. \tag{3}$$

Recognizing that the left-hand side represents the electromotive force induced in each of the N windings and the right-hand side represents the time change in magnetic flux, Φ_B, through the coil, the induced voltage across the Rogowski coil is then

$$U_i = -N\frac{d\Phi_B}{dt}. \tag{4}$$

The measured voltage signal across a current-viewing resistor, R_{CVR}, that is generated by a Rogowski coil with inductance L and a parasitic resistance R can be determined by solving Kirchhoff's voltage law,

$$0 = N\frac{d\Phi_B}{dt} - L\frac{dI_C}{dt} - (R + R_{\mathrm{CVR}})I_C, \tag{5}$$

for the circuit current, I_C, to give

$$I_C + \frac{L}{R + R_{\mathrm{CVR}}}\frac{dI_C}{dt} = \frac{N}{R + R_{\mathrm{CVR}}}\frac{d\Phi_B}{dt}. \tag{6}$$

If the characteristic response time of the circuit is much smaller than the time over which the primary current varies, the second term on the left-hand side of Eq. (6) is much smaller than the first term. As a result, the circuit current, I_C, which generates the measured voltage across the current-viewing resistor, is directly proportional to the time rate of change in the primary current. Therefore, the probe measures changes in current and the signal needs to be integrated. The advantages of these *differentiating* probes are that the coils themselves are straightforward in their construction and produce a relatively high output voltage for a given coil area. The main disadvantage is that the output voltage is frequency-dependent. If instead the Rogowski coil was designed to make the second term larger than the first term, the coil would be *self-integrating*. This design has the advantage that the output voltage is essentially independent of frequency and does not need to be integrated. Unfortunately, the high required inductance, L, makes this design very bulky and thus it is unsuited for positioning inside the plasma gun. Therefore, a differentiating type design was chosen for the described experiments.

When the experiment involves rapidly varying high voltages, as is the case here, a particular concern are signal currents that are generated by electric fields rather than by the time-varying magnetic fields. This electrostatic (or capacitive) pickup is undesirable in a Rogowski coil as it leads to incorrect current measurements. Since electrostatic shielding of the entire assembly is impractical for the described experiment, a better approach is to design the diagnostic circuit to be balanced and then use a differential amplifier to extract the signal.

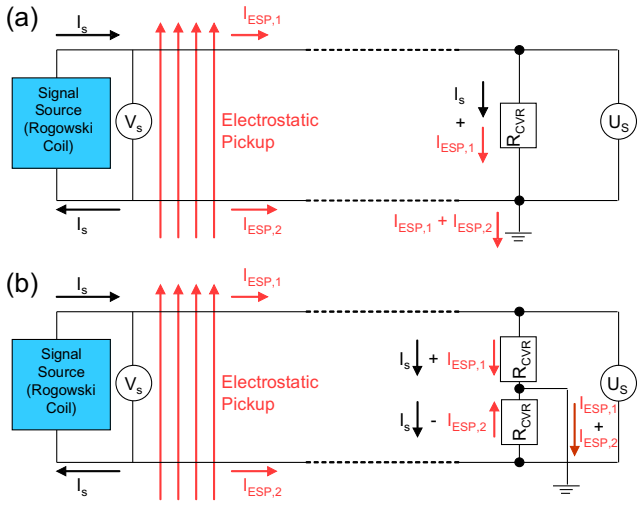

FIG. 5. (Color online) Illustration showing currents induced by electrostatic pickup and how they influence the measured signal voltage, U_S, in an unbalanced circuit (a) and a balanced circuit (b).

In a balanced circuit, electrostatically induced currents face an equal impedance to ground in both of the signal-carrying wires. As a result, the desired signal can be measured as the difference across a load impedance. As is illustrated in Fig. 5, this approach makes use of the fact that electrostatic fields induce currents in the same direction on both wires while the signal from a balanced probe produces equal but opposite currents. This approach is possible because the Rogowski coil itself is a balanced probe.

The challenge is that most experiments generally require the use of unbalanced components, such as coaxial cables, where the outer shield has a different impedance than the inner cable, and oscilloscopes which measure voltage across a load impedance to ground. The transition from a balanced circuit to an unbalanced one can be accomplished through balun transformers or differential amplifiers. The use of differential amplifiers is preferred in this case because the low bandwidth and susceptibility to radiofrequency noise make transformers unsuitable for this application. Since fast differential amplifiers that can measure a small signal on top of a high offset are expensive, a design was chosen that minimizes the electrostatically induced offset voltage so that less expensive differential amplifiers with a low common mode rejection ratio could be used.

IV. DESCRIPTION OF ROGOWSKI COILS

The requirements for the current probes used in the described experiments were accurate current measurements from 100 A to 100 kA, a submicrosecond response time and immunity to electrostatic pickup. To meet these requirements, a dual-Rogowski coil approach similar to the one de-

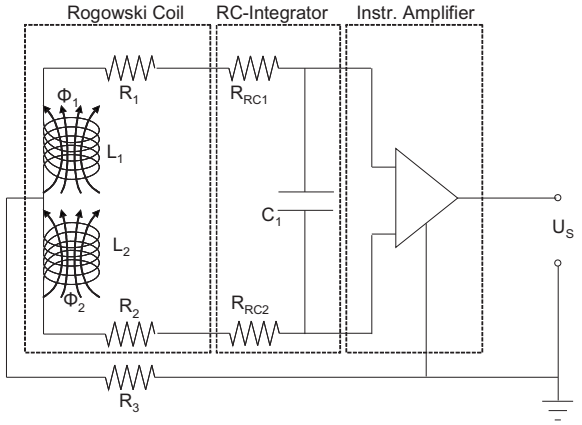

FIG. 6. Circuit diagram of Rogowski coil pair with integrator and differential amplifier circuit.

scribed by Paul *et al.*[26] was used to maximize electrostatic pickup rejection without the need for a high common mode rejection ratio, which would drive up the cost of the differential amplifiers. In this design, the signals from two oppositely wound coils arranged in a balanced configuration are subtracted from one another, thereby canceling the signals from the electric fields and amplifying those from the current-induced magnetic fields. Figure 6 shows the circuit diagram for each of the constructed Rogowski coils and its supporting electronics. The individual components are described in more detail below.

Each individual coil was constructed by winding approximately 130 turns of 26 AWG[27] copper magnet wires tightly around an o-ring of 2 mm width and 2 cm inner diameter. Two oppositely wound coils that were constructed in this manner were then combined in a concentric configuration by placing one coil immediately behind the other one. One end of each coil was then soldered to one 3 m long 26 AWG copper wire that was connected to ground. The other end of each coil consisted of 3 m long 26 AWG wires that were connected to an *RC*-integrator and instrumentation amplifier. Three wires therefore emanated from each pair of coils. These wires were braided to reduce the enclosed magnetic flux and placed inside the copper conduit on which the probes were mounted. Only the first 2 m of the wires were in vacuum and the remaining 1 m was outside of the vacuum feedthrough. The grounded wire that was connected to both coils ensured that the coils were balanced. It also decreased the induced offset voltage from capacitive pickup by providing the lowest impedance path to ground. Its resistance of 0.4 Ω and inductive reactance of approximately 7 Ω are significantly lower than the 1 MΩ input impedance of the differential amplifier. The coil assembly was then placed inside a silicone rubber coated fiberglass sleeve with a dielectric strength of 7 kV.

Each pair of Rogowski coils was connected to an electric circuit that was placed inside a stainless steel box for electromagnetic shielding. It was found that placing each circuit in its own box significantly reduced noise from crosstalk. As shown in Fig. 6, each circuit consisted of two stages. The first stage was a simple *RC*-integrator in which a 1 kΩ resistor was placed in series on each side of a 100 nF capacitor. This configuration ensured that the *RC*-integrator was balanced. The resulting *RC*-time constant of 200 μs was sufficiently large to prevent saturation of the capacitor on the timescales of interest. The voltage across the capacitor was then converted to an unbalanced signal voltage with respect to ground using an inexpensive instrumentation amplifier chip (Analog Devices AD8130). The chip was powered by two 9 V block batteries to provide a floating power source that avoided the introduction of ground loops. The possible signal range thus extended from −9 to +9 V. The specific control circuit that was used to operate the chip was the basic circuit for unity gain as described in the datasheet provided by the manufacturer.

The constructed coils and integrating circuits were calibrated against a commercially available and precalibrated self-integrating Rogowski coil (Pearson Electronics, Model 110). More specifically, one capacitor was connected to the gun using a single transmission line with its return line fed through the array of six coil assemblies and the Pearson probe. This way, each coil assembly was exposed to the same amount of known current. In this configuration, the plasma gun only served the purpose of a fast, high-current switch.

In order to test for electrostatic pickup, an experiment was performed in which two additional coils were positioned at the 20 cm location inside the gun. Neither of these additional coils surrounded the cathode and both of them were plugged using silicone rubber coated fiberglass sleeves so that no current could flow through them. The first control coil was oriented in parallel and the second control coil orthogonally to the regular cathode coil. In this configuration, the two control coils should measure zero current and any detected signal would therefore have to be due to capacitive pickup or a different source of error. The control coils detected no measurable signal, thereby confirming excellent pickup rejection of the Rogowski coils used in these experiments.

V. CURRENT DISTRIBUTION MEASUREMENT

The first configuration investigated was a bank capacitance of 112 μF (eight parallel capacitors) and a transmission line inductance of 50 nH (eight lines in parallel). The applied anode voltage was 1 kV. Figure 7(a) shows the measured cathode currents as they vary with time, following the initial breakdown within the gun. Note the successive delay in current onset for distances along the cathode further from the breech. The current at each axial location consists of the accumulated radial current that entered the cathode at all locations downstream of the probe. Therefore, the difference between measurements from adjacent probes then represents the radial current that entered the cathode between the respective probes at a given time. Figure 7(b) shows this difference, arranged to illustrate the axial distribution of radial currents at different times.

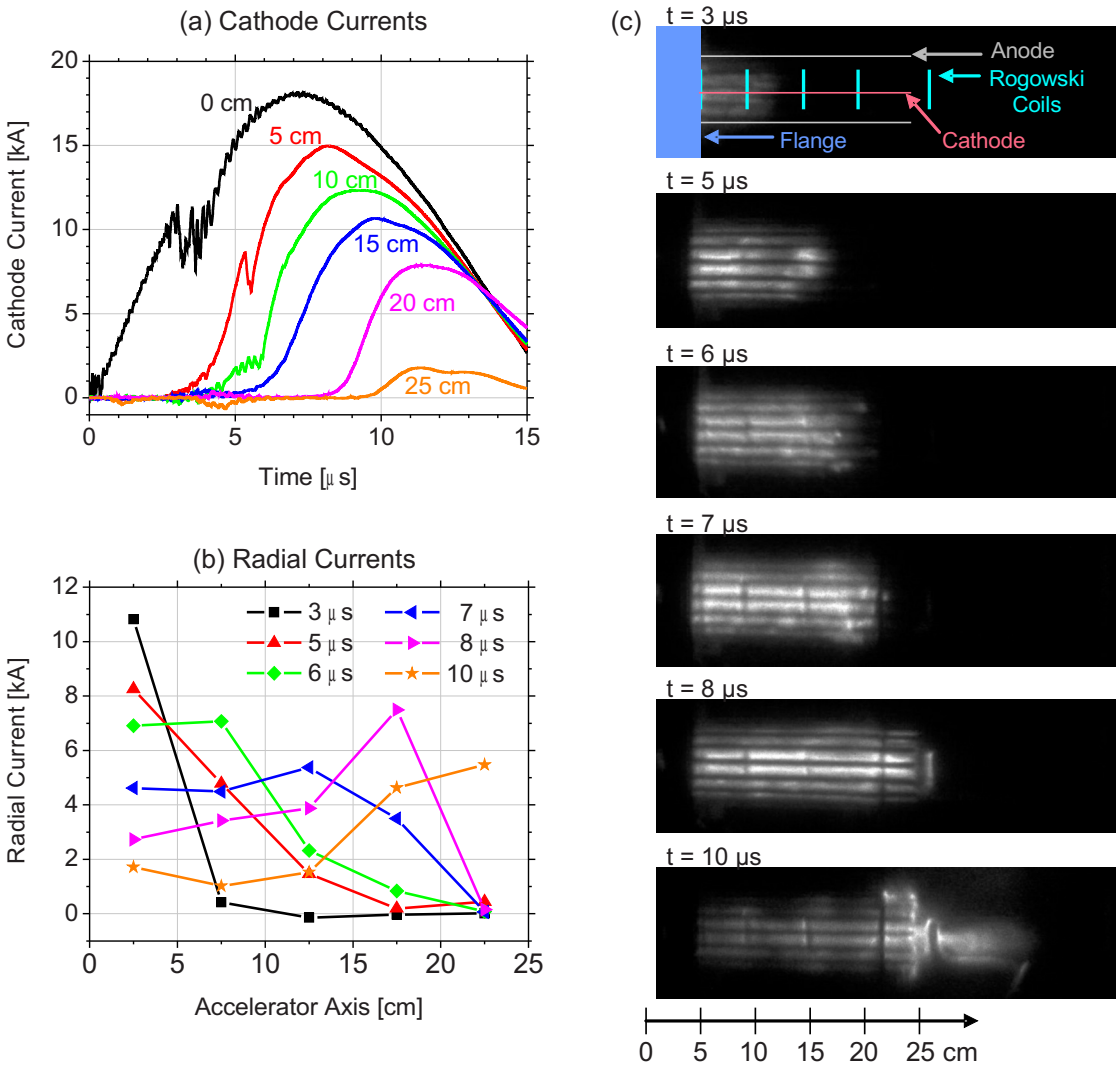

FIG. 7. (Color online) Cathode current at different axial locations (after digital low-pass filtering, $\tau = 1 \times 10^{-7}$ s) (a), corresponding axial distribution of radial currents (b) and fast framing camera images of plasma discharge inside coaxial plasma gun (c) for operation at 1 kV applied anode voltage, eight capacitors (112 μF) and 50 nH transmission line inductance.

The measurements show that the current was concentrated within the first 5 cm of the gas entrance during the first 4 μs of the pulse. During the next 5 μs the current spread along the cathode, and by 7 μs into the discharge, the current was distributed almost uniformly along the first 15 cm of the cathode. This measurement of the current distribution is consistent with the optical emission detected by the fast framing camera images presented in Fig. 7(c). The frame rate and exposure time of the shown image sequence were 2 μs and 100 ns, respectively.

The data in Fig. 7 indicate that the downstream end of the discharge zone was moving at an average speed of approximately 50 km/s. Since no gas was initially present at downstream locations at the time of breakdown, the expansion of the discharge zone must be driven by gas that was accelerated downstream by the deflagration process.

The dips in the signal traces for the measured cathode currents in Fig. 7(a) that are seen at the 0 and 5 cm locations at times $t=3$ μs and $t=5.5$ μs, respectively, can be explained by considering the corresponding images in Fig. 7(c). It appears that during the early stages of the expansion process when the anode voltage is still high, the presence of the coils can facilitate breakdown at a lower density, thereby causing a portion of the current to jump ahead as the density at downstream locations approaches the Paschen breakdown limit. This sudden change in inductance causes a brief transient in the measured current at upstream locations. Alternatively, the sudden change in inductance could also be caused by a local recompression of the axial current distribution. However, the first explanation appears more plausible as the current dip on both the 0 and 5 cm coils coincides with the sudden rise in current at the adjacent downstream probe.

VI. PARAMETER VARIATION

Three series of experiments were performed to understand how the main circuit parameters (bank capacitance, transmission line inductance, and applied anode voltage) influence the operation of the plasma gun. In each series, one

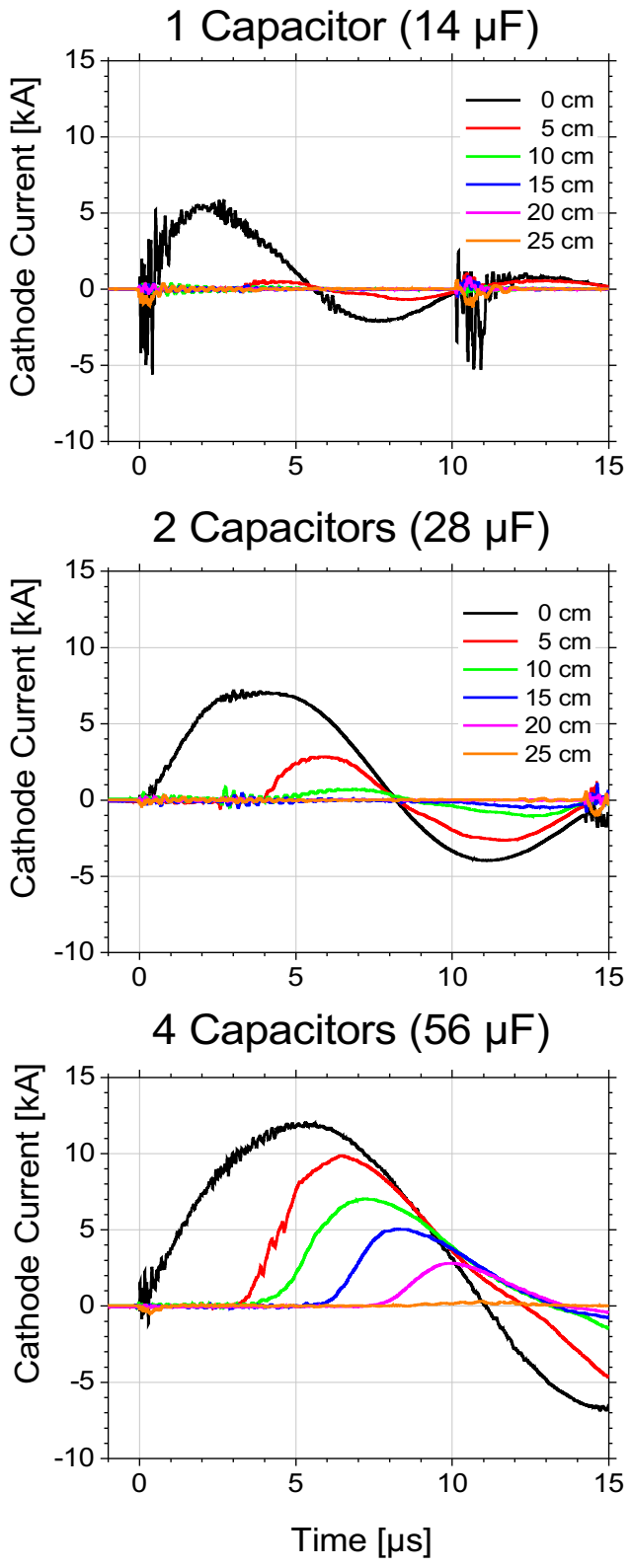

FIG. 8. (Color online) Effect of bank capacitance on cathode current at different axial locations for operation at 1 kV applied anode voltage and 50 nH transmission line inductance. Digital low-pass filter: $\tau = 1 \times 10^{-7}$ s.

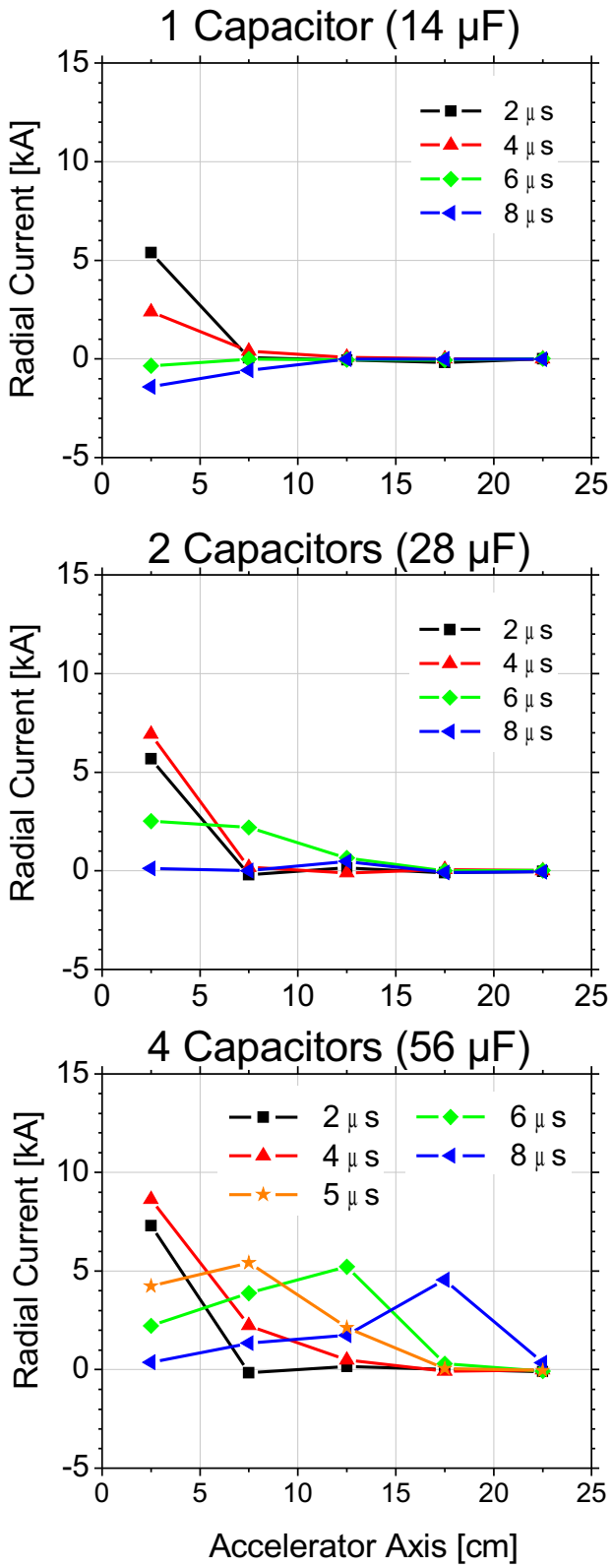

FIG. 9. (Color online) Effect of bank capacitance on axial distribution of radial currents for operation at 1 kV applied anode voltage and 50 nH transmission line inductance.

of the circuit parameters was varied while all others were kept constant. The radial current distribution was measured using the Rogowski coil array. The results are presented below.

A. Capacitance

The bank capacitance was varied to include operation with one, two, and four capacitors, in addition to the case with eight capacitors shown in Fig. 7. As before, the com-

TABLE I. Summary of effect of bank capacitance on plasma gun operation at 1 kV applied anode voltage and 50 nH transmission line inductance.

Number of capacitors	1 (14 μF)	2 (28 μF)	4 (56 μF)	8 (112 μF)
Half-cycle period (μs)	6	8	12	16
Peak cathode current (kA)	5	7	12	18
Axial extent of discharge (cm)	5	10	20	20

bined transmission line inductance was 50 nH. The applied anode voltage was 1 kV. The results are shown in Figs. 8 and 9 and Table I.

The period of the first half-cycle of the discharge pulse was found to increase from approximately 6 μs for operation with one capacitor to 8 μs for two capacitors, to 12 μs for four capacitors, and to 16 μs for eight capacitors. This agrees well with the expected $\sqrt{C}$ dependency of the LC-time constant. In addition, one can see from Fig. 8 that the peak cathode current at the cathode base increased from 5 kA for one capacitor to 7 kA for two capacitors, to 12 kA for four capacitors, and to 18 kA for eight capacitors. Since the total charge that is stored in the capacitor bank scales linearly with the bank capacitance (at a fixed voltage) and the time during which this charge is discharged scales with $1/\sqrt{C}$, it is expected that the peak current also scales with $\sqrt{C}$. This appeared to be approximately the case, although the measured peak currents exceeded the expected values by up to 20% at the higher capacitance configurations. As described later, this discrepancy is most likely due to a drop in effective gun inductance as the current distribution inside the gun becomes more diffuse. The axial extent to which the current conduction region spreads during the first half-cycle of the discharge increases with bank capacitance. For operation with only one capacitor, the current conduction region is confined within the first 5 cm of the gun axis. When operated with two capacitors this region spreads to 10 cm and eventually to the entire length of the gun when operated with four or more capacitors. This also agrees well with theoretical expectations for two reasons. First, the longer LC-time constant gives the plasma more time to spread downstream, and second, the higher currents and resulting stronger $J \times B$ forces cause the plasma to spread downstream at a faster rate.

B. Inductance

The transmission line inductance was varied by placing different numbers of 1.75 m long RG-8 coaxial transmission line cables in parallel. The cathode currents were measured for configurations using two, four, or eight cables, corresponding to combined transmission line inductances of 200, 100, and 50 nH, respectively. In all cases, two capacitors were used, resulting in a bank capacitance of 28 μF and the applied anode voltage was 1 kV. The results are shown in Figs. 10 and 11 and Table II.

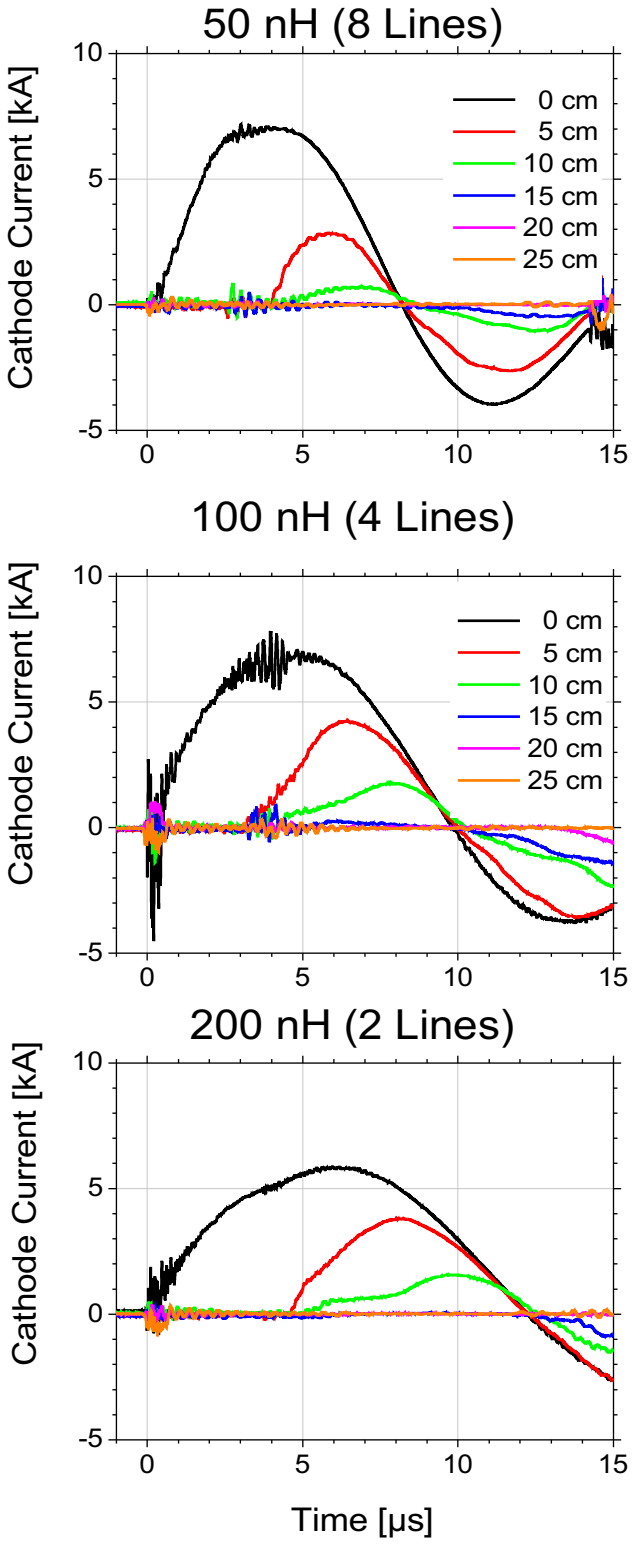

FIG. 10. (Color online) Effect of transmission line inductance on cathode current at different axial locations for operation at 1 kV applied anode voltage and two capacitors (28 μF). Digital low-pass filter: $\tau = 1 \times 10^{-7}$ s.

The period of the first half-cycle of the discharge pulse was found to increase from 8 to 10 μs, and then to 12 μs as the transmission line inductance was increased. This increase in half-cycle time was well below the expected $\sqrt{L}$ dependency of the system LC-time constant, indicating that the

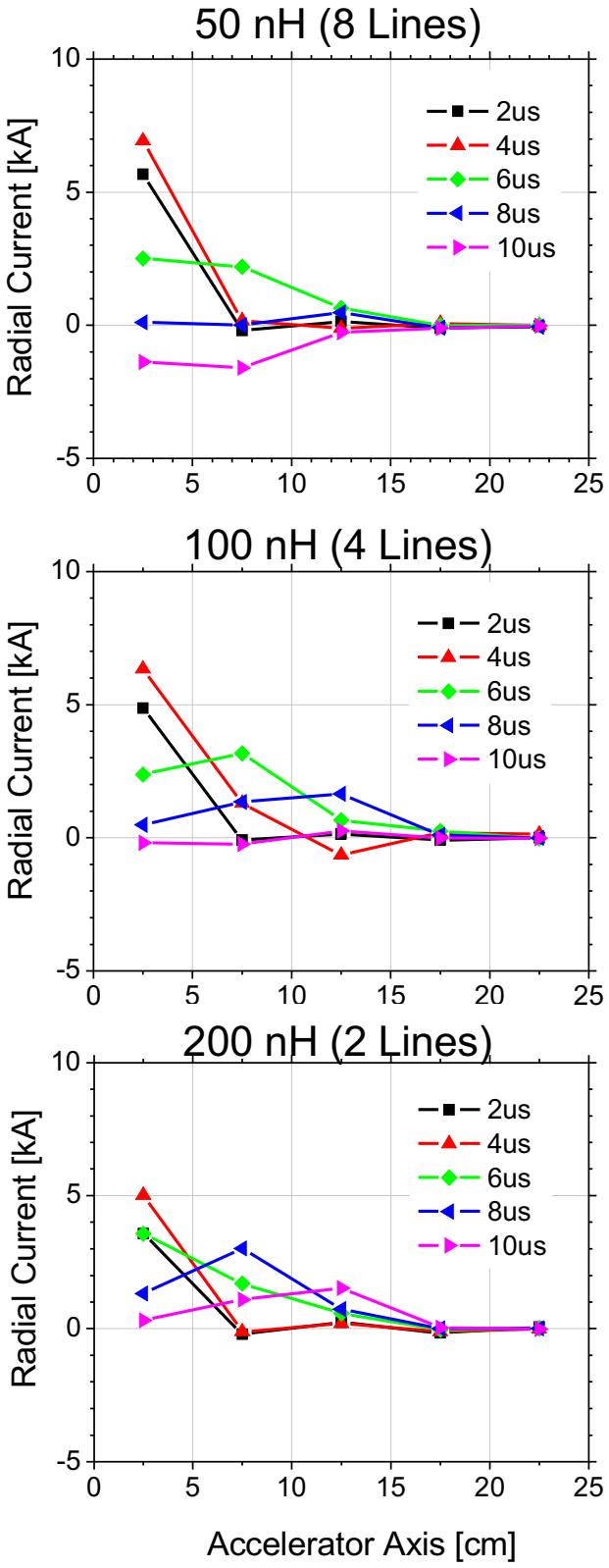

FIG. 11. (Color online) Effect of transmission line inductance on axial distribution of radial currents for operation at 1 kV applied anode voltage and two capacitors (28 μF).

inductance in other parts of the circuit was comparable to that of the transmission lines.

Similarly, the peak cathode current at the cathode base increased only slightly from 6 to 7 kA as the transmission line inductance was reduced from 200 to 100 nH. This small increase is consistent with expectations as the charge stored in the capacitors is not changed by the inductance and the time over which this charge was discharged decreased only slightly. When the number of transmission lines was further increased to 8, no noticeable difference in peak cathode current was observed, despite the further reduction in half-cycle time. The 0 cm waveform (Fig. 10), however, appeared less sinusoidal than before, and, while the peak current did not increase, the duration of the peak did. This indicates that the time-dependent electrical properties of the plasma are behaving differently in the two cases.

In addition, the axial extent to which the current conduction region spread during the first half-cycle of the discharge appeared to vary little with the transmission line inductance. For all three configurations the axial extent ranged between 12 and 15 cm. This is consistent with expectations as a reduction in inductance increases the $J \times B$ force which spreads the plasma downstream, but also reduces the duration of the first half-cycle, giving the plasma less time to spread downstream. These two effects therefore partly counteract one another as the transmission line inductance is changed.

TABLE II. Summary of effect of transmission line inductance on plasma gun operation at 1 kV applied anode voltage and two capacitors (28 μF).

Transmission line inductance (lines) (nH)	50 (8)	100 (4)	200 (2)
Half-cycle period (μs)	8	10	12
Peak cathode current (kA)	7	7	6
Axial extent of discharge (cm)	12	15	15

C. Voltage

The applied anode voltage was varied in 1 kV increments from 1 to 3 kV. In all cases, one capacitor and eight transmission lines were used, resulting in a bank capacitance of 14 μF and a transmission line inductance of 50 nH. The results are shown in Figs. 12 and 13 and Table III.

The period of the first half-cycle of the discharge pulse was found to decrease slightly from 6 to 5.8 μs and finally to 5.3 μs as the voltage was increased. Since the period in an *LC*-circuit is independent of voltage, the period of the half-cycle was expected to remain constant. However, the axial extent of the discharge increased monotonically with the applied voltage as the $J \times B$ force increases. This broadening of the discharge has the same effect as placing additional conductors in parallel and thus results in a decreasing impedance of the plasma as the pulse progresses, thereby explaining why the half-cycle period dropped with higher applied voltages.

The peak cathode current appears to scale almost linearly with the applied voltage. This is in good agreement with expectation since the charge stored in the capacitor depends linearly on voltage, and the time over which the capacitors are discharged changed only slightly.

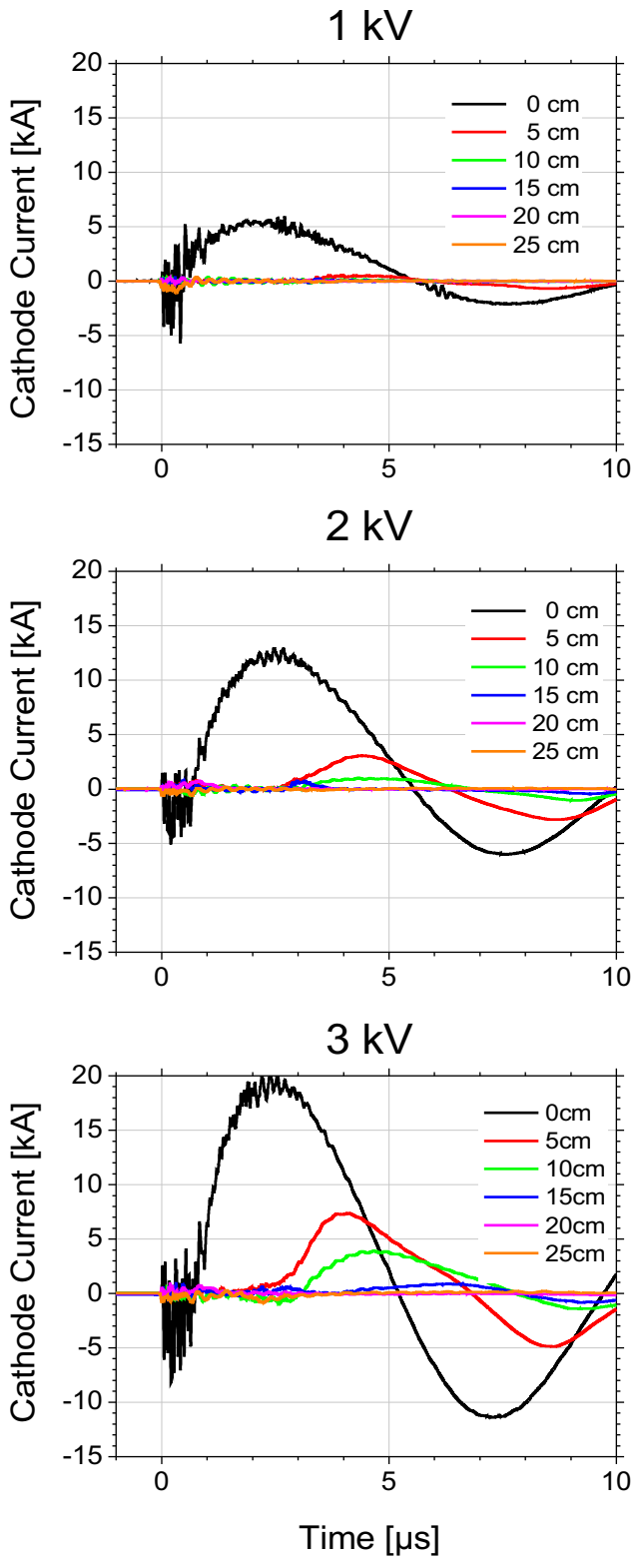

FIG. 12. (Color online) Effect of applied anode voltage on cathode current at different axial locations for operation with one capacitor (14 μF) and 50 nH transmission line inductance. Digital low-pass filter: $\tau = 1 \times 10^{-7}$ s.

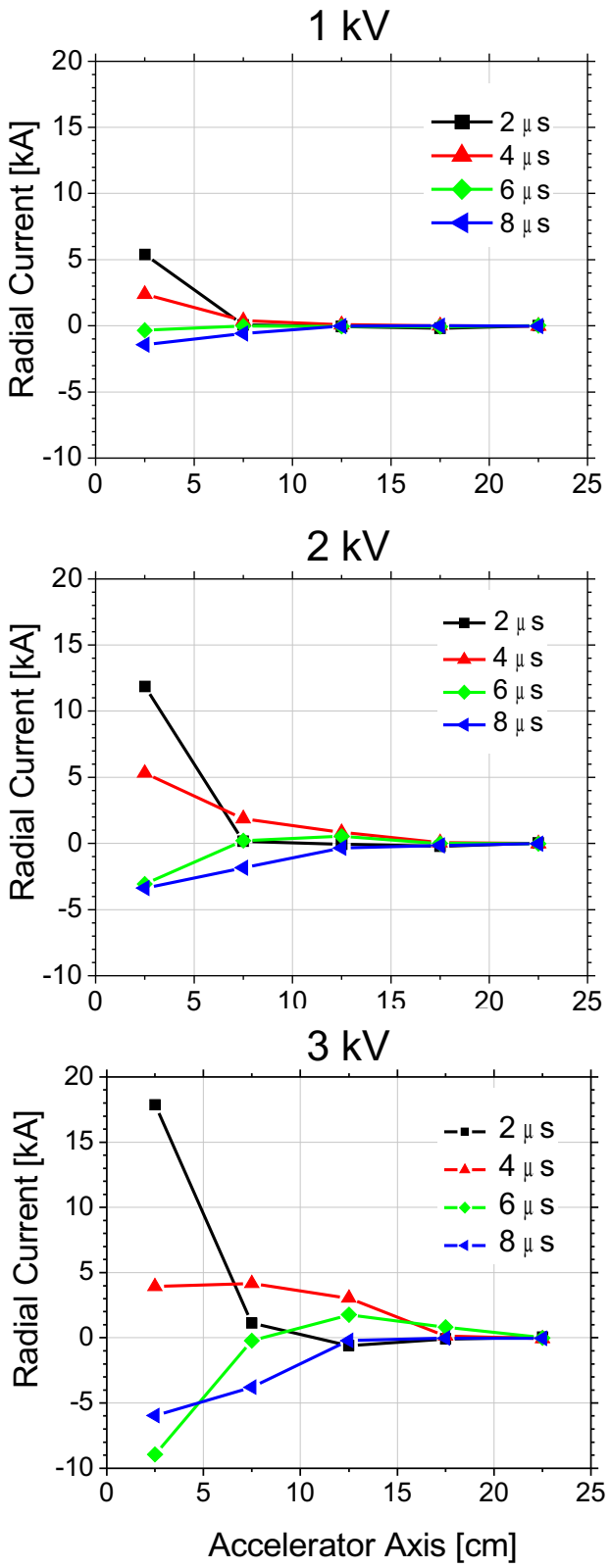

FIG. 13. (Color online) Effect of applied anode voltage on axial distribution of radial currents for operation with one capacitor (14 μF) and 50 nH transmission line inductance.

It is also noteworthy that at higher discharge voltages a portion of the radial current continues to flow radially inward, even after the current has already reversed at the gun breech. This is particularly visible at $t = 6$ μs of the 3 kV case, where a diffuse radial current of approximately 3 kA continues to enter the cathode at downstream locations between 7.5 and 17.5 cm. Such *self-crowbar* discharges are not uncommon in coaxial plasma guns, particularly those oper-

TABLE III. Summary of effect of applied anode voltage on plasma gun operation with one capacitor (14 μF) and 50 nH transmission line inductance.

Applied anode voltage (kV)	1	2	3
Half-cycle period (μs)	6	5.8	5.3
Peak cathode current (kA)	6	12.5	19
Axial extent of discharge (cm)	5	15	17.5

ating in a snowplow mode.[28] Future experiments will further examine these higher voltage conditions where self-crowbar discharges are of particular interest, as these crowbars isolate the magnetic energy stored in the plasma from the driving capacitor bank.

VII. SUMMARY

Studies were carried out of a pulsed coaxial discharge operating in a gas-puff mode, i.e., where the voltage across the electrodes is applied prior to filling of the gun with gas from the breech end. An array of Rogowski coil assemblies was successfully immersed into the plasma without detecting interference from electrostatic pickup. The coils were axially distributed along the central cathode, with the difference in current detected between adjacent coils representing the radial discharge current between these coils. The measured radial current distributions were compared to high speed images, acquired simultaneously, of the optical emission from the interior of the gun. The axial expansion of current-carrying plasma was consistent with the expansion of the light-emitting region in the camera images. The obtained data confirmed that the gas-puff method of operation leads to a plasma deflagration, even with operating voltages as low as 1 kV. This was evidenced by a stationary ionization front that was followed by plasma acceleration in the downstream direction. Effects of varying the bank capacitance, transmission line inductance, and applied anode voltage on peak currents and pulse durations were largely consistent with expectations for the behavior of a standard *LC*-circuit. In addition, the axial extent of the discharge during the first half-cycle of a pulse scaled with the *LC*-time constant and the $J \times B$ force. It is noteworthy, however, that the effect of the axial spreading of the discharge was large enough to alter the overall circuit dynamics through temporal evolution of the discharge impedance. We see that at higher bank discharge voltages, a self-crowbar discharge develops at the gun breech, as is often seen in similar coaxial guns that operate in a snowplow mode.[28] Future experiments will examine further the detailed structure of the plasma as it develops in this self-crowbar deflagration mode regime.

ACKNOWLEDGMENTS

We are grateful to Dr. Dah Yu Cheng for his donation of pulsed power equipment for the plasma gun facility and for some stimulating discussions in the early phases of this work. This research was partially supported by the National Institutes of Health (Grant No. 1 R21 CA139320-01), the Stanford Graduate Fellowship, and the Air Force (Contract No. FA9550-08-C-0099, STTR sub-contract through Busek Co.).

[1] A. W. Leonard, R. N. Dexter, and J. C. Sprott, Phys. Rev. Lett. **57**, 333 (1986).
[2] S. F. Schaer, Acta Phys. Pol. A **88**, S-77 (1995).
[3] S. Woodruff, D. N. Hill, B. W. Stallard, R. Bulmer, B. Cohen, C. T. Holcomb, E. B. Hooper, H. S. McLean, J. Moller, and R. D. Wood, Phys. Rev. Lett. **90**, 095001 (2003).
[4] A. Bernard, P. Cloth, H. Conrads, A. Coudeville, G. Gourlan, A. Jolas, Ch. Maisonnier, and J. P. Rager, Nucl. Instrum. Methods **145**, 191 (1977).
[5] J. W. Mather, Phys. Fluids **7**, S28 (1964).
[6] F. Castillo Mejía, M. Milanese, R. Moroso, and J. Pouzo, J. Phys. D **30**, 1499 (1997).
[7] K. Masugata, Y. Kawahara, C. Mitsui, I. Kitamura, T. Takahashi, Y. Tanaka, H. Tanoue, and K. Arai, *Conference Record of the 25th International Power Modulator Symposium and 2002 High-Voltage Workshop*, Hollywood, CA, 2002, edited by L. Gordon (IEEE, Piscataway, NJ, 2003), p. 334.
[8] P. Yan, P. Hui, W. Zhu, and H. Tan, Surf. Coat. Technol. **102**, 175 (1998).
[9] M. -Y. Wang, C. K. Choi, and F. B. Mead, Jr. , AIP Conf. Proc. **246**, 30 (1992).
[10] D. Y. Cheng, AIAA J. **9**, 1681 (1971).
[11] J. T. Cassibry, Y. C. F. Thio, and S. T. Wu, Phys. Plasmas **13**, 053101 (2006).
[12] P. J. Hart, J. Appl. Phys. **35**, 3425 (1964).
[13] T. D. Butler, I. Henins, F. C. Jahoda, J. Marshall, and R. L. Morse, Phys. Fluids **12**, 1904 (1969).
[14] D. Y. Cheng, Nucl. Fusion **10**, 305 (1970).
[15] D. M. Woodall and L. K. Len, J. Appl. Phys. **57**, 961 (1985).
[16] D. C. Black, R. M. Mayo, and R. W. Caress, Phys. Plasmas **4**, 2820 (1997).
[17] T. E. Markusic, E. Y. Choueiri, and J. W. Berkery, Phys. Plasmas **11**, 4847 (2004).
[18] Although the specific forces associated with blowby (e.g. radial variation in magnetic pressure) are likely to be present in the deflagration mode as well, their overall effect may be less relevant since the upstream end of the current conduction region is stationary at the gun breech and continuously feeds on incoming neutral gas. Therefore the path of current conduction may not be as intrinsically linked to the motion of the accelerated ions as in the snowplow mode.
[19] R. L. Byer and M. D. Duncan, J. Chem. Phys. **74**, 2174 (1981).
[20] A. P. Chattock, Philos. Mag. **24**, 94 (1887).
[21] W. Rogowski and W. Steinhaus, Arch. Electrotech. **1**, 141 (1912).
[22] E. S. Wright, Guggenheim Laboratories for the Aerospace Propulsion Sciences Report No. 740, 1965.
[23] F. Piperno and G. Solaini, Nuovo Cimento B **29**, 239 (1975).
[24] D. G. Pellinen, M. S. Di Capua, S. E. Sampayan, H. Gerbracht, and M. Wan, Rev. Sci. Instrum. **51**, 1535 (1980).
[25] P. E. Stott, *Course on Plasma Diagnostics and Data Acquisition Systems*, Varenna, Italy, 1975 (Editrice Compositori, Bologna, 1975), p. 1, Paper No. A76-41027 20-75.
[26] M. K. Paul, P. K. Chattopadhyay, and D. Bora, Meas. Sci. Technol. **18**, 2673 (2007).
[27] American Wire Gauge
[28] C. J. Michels, NASA Technical Report No. TN D-2571, 1964.